Nuclear Instruments and Methods in Physics Research A306 (1991) 474–484
North-Holland

The optimization of the electrostatic field inside the ZEUS forward drift chambers: calculations and measurements

M.P. Dobberstein [1]
Bonn University, Germany

F. Krawczyk [2] and M. Schäfer-Jotter [3]
TH Darmstadt, Germany

Received 4 March 1991

The electrostatic field inside small drift cells shows in general edge effects which are not negligible. These are usually corrected by field-shaping wires or strips. The operating voltages of the field-shaping electrodes have to be adjusted to maximize the field homogeneity. We present the underlying ideas of such an optimization procedure for the cells of the ZEUS forward drift chambers. Using the finite difference code PROFI, the optimization can be performed automatically by a multiple solution of the Poisson equation. An experimental verification of the optimal voltages was carried out by measuring the gas amplification at the six sense wires. Modifications of the drift cell geometry were necessary for calibration measurements with a laser beam. This caused additional distortions of the electrostatic field. Their influence was calculated using the MAFIA code, which allows to include open boundary conditions.

1. Introduction

1.1. General introduction

The ZEUS detector is one of the high energy physics experiments at the electron proton storage ring HERA at DESY in Hamburg [16]. This detector is designed to take into account the spatially asymmetric interactions between the electrons and the much heavier protons. It has special drift chambers in the proton forward direction (the forward tracking devices, FTD = FTD1 + FTD2 + FTD3) and smaller ones in the electron forward direction (the rear tracking device, RTD).

These drift chambers are placed at the ends of the superconducting solenoid and therefore are operated in a high (up to 1.5 T) and strongly inhomogeneous (maximum field gradient 2–3 T/m) magnetic field, see fig. 1. This has consequences for the FTD/RTD drift chambers, as explained in section 1.2.

The investigations presented in this paper were performed in connection with the calibration of the FTD/RTD, as outlined in ref. [3]. The procedure for the automatic field optimization was developed in ref. [12] and the field calculations with open boundary conditions are based on the algorithms shown in ref. [6].

1.2. The design of FTD / RTD and the optimization of its operating voltages

To reduce [#1] the influence of the magnetic field gradient, the FTD/RTD is divided in small cells with inner dimensions 24 mm × 48 mm, having seven potential and six sense wires each. Thus inside one 2D cell section (cf. fig. 2) the variation of the magnetic field is kept small, which is important to achieve a similar behaviour of the six sense wires inside one cell. Besides the six sense wires, each cell contains seven potential wires, two sets of five field-shaping strips, and two cathode planes. The cell lengths in the z direction vary from about 30 up to about 215 cm (see fig. 2 for the coordinate system conventions, which differ from the global ZEUS coordinates shown in fig. 1). The walls are made of dielectric ($\epsilon_r = 4$) G10 epoxy material of thickness 1 mm.

The small extent of the cells causes new problems with respect to the electrostatics: To avoid edge effects

[1] Now at DESY, Notkestrasse 85, 2000 Hamburg 52, Germany.
[2] Fachgebiet Theorie Elektromagnetischer Felder (FB 18), Schlossgartenstr. 8, 6100 Darmstadt, Germany.
[3] Now at Kuhnke GmbH, Lütjenburgerstr. 101, 2427 Malente, Germany.

[#1] This is only one of the reasons for the cell design.

0168-9002/91/$03.50 © 1991 – Elsevier Science Publishers B.V. (North-Holland)

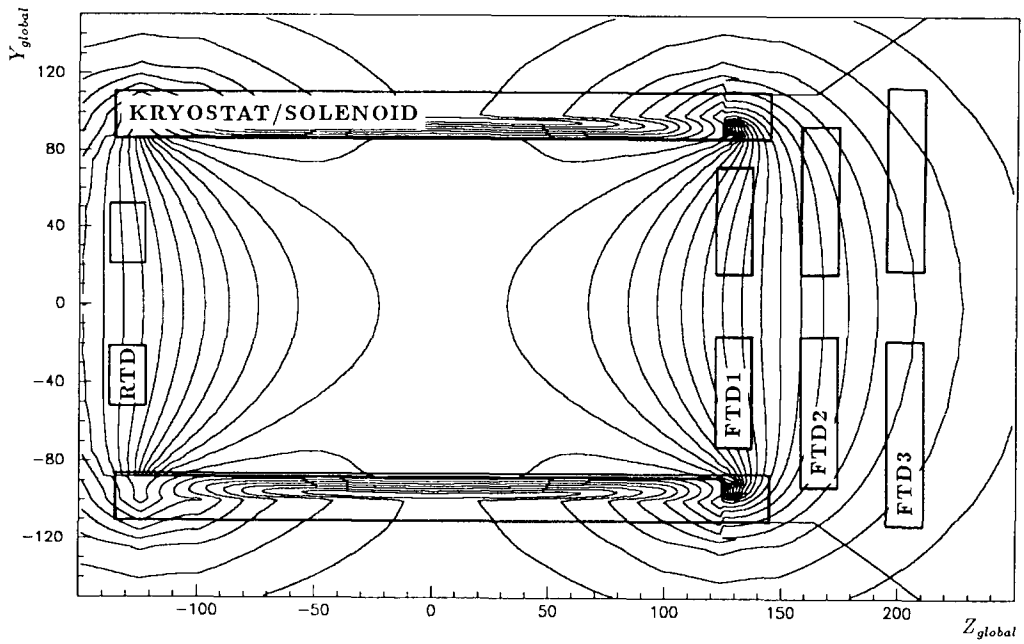

Fig. 1. The position of the FTD/RTD drift chambers inside the ZEUS detector (the axes are labeled in units of cm). Also shown are lines of constant absolute value of the magnetic field.

one has to use the field-shaping strips (see fig. 2) and then find the "right" operating voltages for these strips. The shape of the drift trajectories at sense wires 1 and 6 is strongly influenced by the choice of the strip voltages. In fig. 3 one sees the result of a calculation [3,2] of the drift trajectories inside a FTD/RTD cell section for nonoptimized voltages at the strips; in contrast, in fig. 4 the calculated trajectories are shown for optimized voltages (both without a magnetic field). In the second case the drift trajectories are more uniform, simplifying the calibration of the drift chamber. We therefore define a set of strip voltages to be optimal if there is (within the desired resolution of the drift chamber) no measurable difference between the drift times on sense wire 1 and sense wire 3 (see section 2.2 for details).

Things become more complicated in the presence of

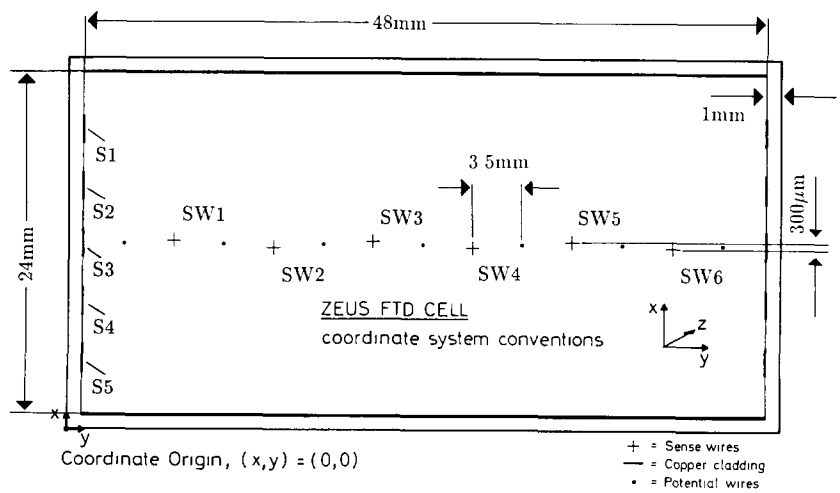

Fig. 2. A two-dimensional cross section of a FTD/RTD cell. The six sense wires are denoted by SW1,...,SW6, the field-shaping strips by S1,...,S5

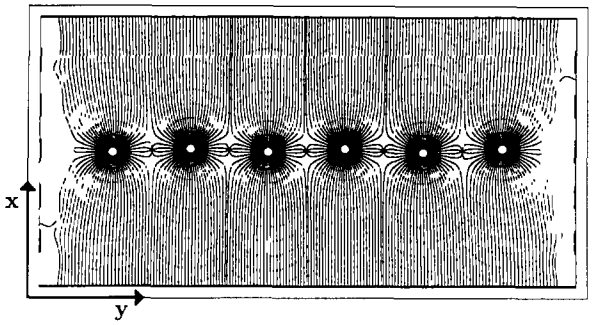

Fig. 3. The drift trajectories inside a FTD/RTD cell section for nonoptimized voltages of the field-shaping strips (no magnetic field).

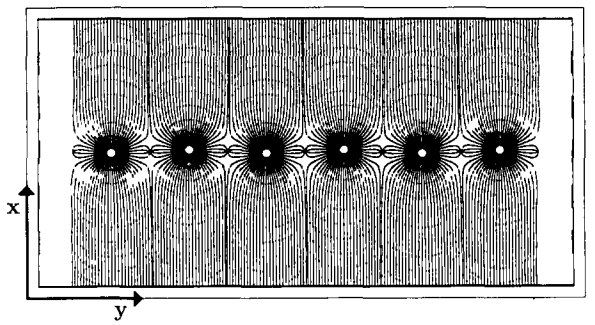

Fig. 4. The drift trajectories inside a FTD/RTD cell section for optimized voltages of the field-shaping strips (no magnetic field).

a magnetic field. One can see this in fig. 5, where for the same voltages as in fig. 4 a magnetic field of $B = (0.0, -13.1, 5.7)$ kG, which is typical for FTD1, was applied. The two 2D projections show electron drifts in space and have, despite the optimal strip voltages, an abnormal shape of the trajectories at the sense wires 1 and 6. These effects are not negligible within the resolution of the drift chamber designed at 100 μm.

1.3. The design of the laser test cell and the differences between the test cell and the original cell

For calibration measurements a laser test cell was built [3,4,14]. Besides the short cell length (about 12 cm), the main difference between the original cell and the final FTD/RTD cell was a laser window of size 2 mm × 24 mm (see fig. 6). This window is of the same order of magnitude as the 2D cell section and is located where the ionization process takes place. The question then arises whether the measurements are affected by the disturbances of the cell electrostatics caused by the laser window. To clarify this, 3D calculations of the electrostatic field of the laser test cell were performed, incorporating the open boundary conditions of the laser window.

An older version of the laser test cell (with a window of another shape) is of interest for comparisons. This cell is not described in this text, but cited sometimes as "the old laser cell". See ref. [3] for details.

1.4. The relation between optimal voltages and gas amplification

The optimal voltages are defined in section 2.2 precisely via asymmetries of drift times. The direct experimental verification of optimal voltage settings according to this definition is expensive because one has to measure drift times at two angles aligned very accurately relative to one other. Therefore another criterion seems to be more suited to detect optimal voltages: The gas amplification at a sense wire depends exponentially on the electrostatic surface field at the wire (see ref. [10] for details). Since the surface fields at sense wires 1 and 6 are directly related to the voltages applied to the field-shaping strips (optimal voltages are equivalent [#2] to identical surface fields at all sense wires 1,...,6), the measurements of the gas amplification and the compari-

[#2] This was established with our numerical studies.

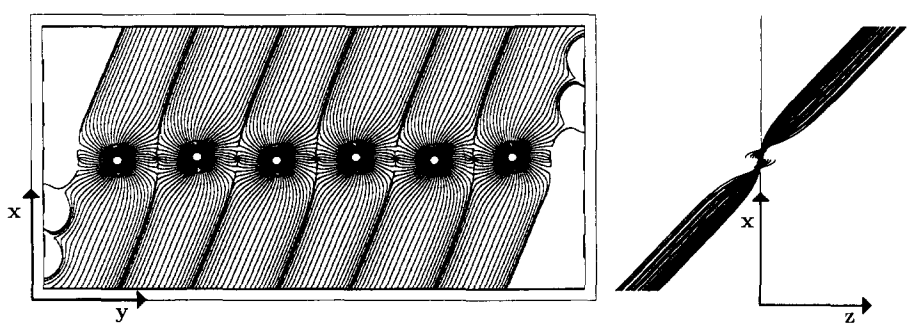

Fig. 5. The drift trajectories inside a FTD/RTD cell section for optimized voltages of the field-shaping strips and a magnetic field of $B = (0.0, -13.1, 5.7)$ kG.

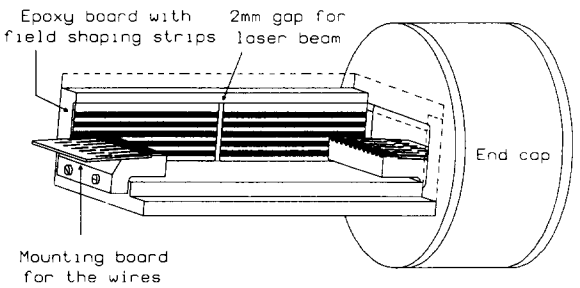

Fig. 6. A sketch of the laser test cell.

son is a good tool to check the voltage optimization experimentally.

For our drift chambers a variation of the surface fields in the order of 1% implies a variation of the gas amplification in the order of 10–15%. Therefore, an experimental error of 10% in the measurements of the (relative) gas amplification is sufficient to detect differences of 1% in the surface fields. Related to this one has to know that for optimal voltages as in fig. 4 the difference between the surface fields at sense wire 1 and sense wire 3 is lower than 0.1% of the field at wire 1, whereas for the nonoptimized voltages of fig. 3 the difference amounts to about 3%.

2. The calculation and optimization of the electrostatic field

2.1. Description of the methods / programs used and some results

Because of the dielectric wall material and the field-shaping strips the standard design-programs for drift chambers could not be applied. Instead, finite difference codes, namely, the programs PROFI [7] and MAFIA [5], were used to model the electrostatic field. For these calculations the cells have been modelled on Cartesian grids covering a 2D cell cross section of the FTD/RTD or a full (3D) cell.

The logarithmically divergent potential near the sense wires requires a very fine grid close to these wires (see fig. 7) to reach a sufficient accuracy in the calculation of the surface fields. The smallest distances between the grid lines have been chosen as 1 μm, and the largest are of the order of magnitude of several 100 μm. Some of the practical problems which arise in dealing with the resulting large and nonequidistant grids are discussed in refs. [1] and [3].

2.1.1. Calculations in two dimensions

The small cross section compared to the length of the FTD/RTD cells actually used in the detector allows to restrict the calculation of the electric field to a 2D cross section of a cell (assuming an infinite length). See

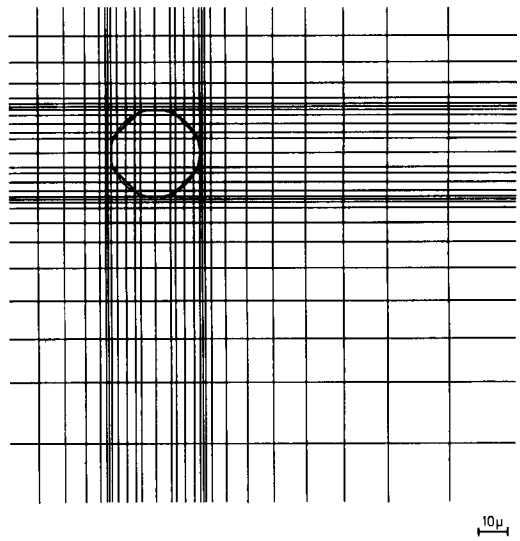

Fig. 7. A typical grid around a sense wire.

figs. 3 and 4 for the drift trajectories inside such a section, which correspond to the electric field lines in the absence of a magnetic field.

These calculations were performed using the widely distributed program package PROFI [7] running on the IBM 3090's at the TH Darmstadt [12,13] and at DESY [8,1]. PROFI is able to solve electrostatic, magnetostatic and related problems in two and three dimensions. Using symbolic input and output, it allows to formulate an optimization problem.

Grids with up to 500 000 nodes, which translates to memory regions of about 40 Mbytes, were used during the execution of a typical job. Clearly, these large grids were only used for the final, accurate calculations. The optimization problem was solved on coarser grids.

To illustrate the 2D field calculation, the influence of the dielectric wall material on the electrostatic field and subsequently on the drift trajectories and drift times shall be demonstrated. In fig. 4 the development of the drift trajectories without a magnetic field is displayed. If the dielectric wall material is "switched off" ($\epsilon_r = 4 \rightarrow \epsilon_r = 1$) one gets the trajectories shown in fig. 8. At wires 1 and 6 the results clearly deviate from the calculations with dielectrics. Quantitatively, the drift times differ by about 4.4 ns at wires 1 and 6, whereas the differences of 0.4 ns at wires 3 and 4 are much smaller (maximum values). Assuming a drift velocity of 51.7 μm/ns for the gas mixture used, argon/ethane (50/50), this is not negligible within the chamber resolution aimed at 100 μm. With a realistic magnetic field, these differences are still larger.

2.1.2. Calculations in three dimensions

Due to the lack of direct incorporation of open boundary conditions the 3D calculations of the electro-

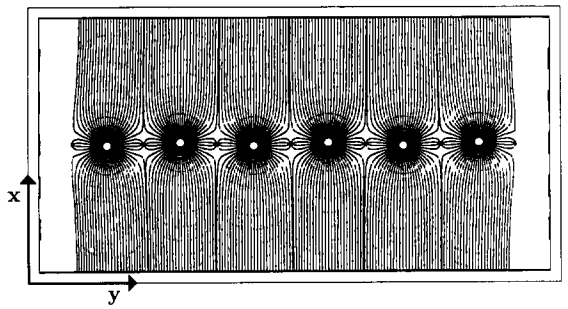

Fig. 8. The drift trajectories inside a FTD/RTD cell section for optimized voltages of the field-shaping strips without the dielectric wall material (no magnetic field).

static field of the laser test cell were not performed with PROFI. Instead the program package MAFIA [5,6] was used. The program has the additional advantage of a high degree of vectorization. This made its usage on the CRAY Y-MP of the Höchstleistungsrechenzentrum (HLRZ) at the Forschungsanlage KFA, Jülich, very efficient. Execution speeds of up to 160 Mflops were achieved using memory regions of up to 80 Mbytes.

Referring to the 2D calculation in fig. 9 the behaviour of the drift time along wire 1 is shown. At the middle of the cell ($z = 60$ mm), where the laser window is placed, one has a maximum deviation of about 4.5 ns between the 2D and 3D calculations (without a magnetic field). For the old version of the laser cell, this difference was significantly larger (up to 9.5 ns), caused by a more poorly chosen shape of the window. Again, with a magnetic field, these differences are much larger.

One gets an idea of the border effects which arise at the end of each FTD/RTD cell, not only inside the laser cells, at $z = 0$, where the wires end.

In addition to the drift times, in fig. 9 the variation of the surface field along wire 1 can be seen. A slight increase is visible close to the laser window. This has to be kept in mind for comparison with the measurements (see section 4). Again, the old laser test cell shows a larger deviation from the 2D case (up to about 3%).

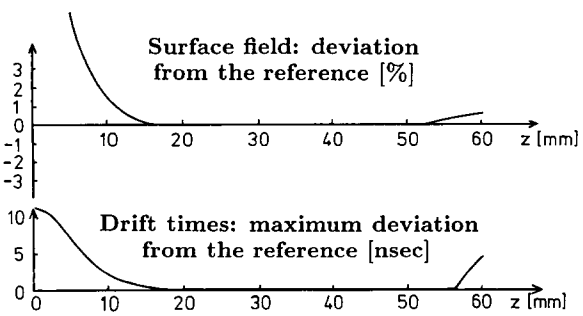

Fig. 9. The deviation of the surface field and of the drift time from the 2D reference, shown along wire 1 of the laser test cell (without magnetic field).

2.2. Voltage optimization "by hand"

From the point of view of the user of drift chambers the voltages at the field-shaping strips are optimal if the drift process behaves identically at all sense wires. This can be understood looking at fig. 10: Using an optimized and a nonoptimized electric field the drift trajectories inside a FTD/RTD cell section were calculated. Also visible are the isochronous lines, i.e. the lines of equal drift times to the corresponding sense wire. Obviously, for nonoptimized strip voltages the trajectories and the isochronous lines at wire 1 are deformed. To record this more quantitatively, two incident tracks with the same distance to the plane of the potential wires (10 mm, measured against sense wire 1), but with opposite angles of incidence ($+30°$ and $-30°$) are considered. Only for optimized voltages the distances to the closest isochronous line are equal. Therefore, the measured drift times are generally different for the two incident tracks. The *asymmetry* is defined by

$$\textit{asymmetry} = |\text{drift time}\,(+30°) - \text{drift time}\,(-30°)|.$$

One can easily imagine that even for nonoptimized voltages this asymmetry vanishes at the inner sense wires 3 and 4, where no deformations occur, but is large at sense wires 1 and 6.

With the asymmetry as the criterion for the quality of the strip voltages, a "by hand" optimization of the voltages can be performed by repeating the following scheme:

1. Calculation of the 2D electric field inside a FTD/RTD cell for given voltages of the sense wires, potential wires and field-shaping strips.
2. Computation of the drift trajectories for the calculated electric field and determination of the asymmetries at the different sense wires.
3. Modification of the strip voltages to reduce the asymmetries.

By definition, the electric field reaches an optimal state, when the asymmetry is at its minimum value on all sense wires. This definition couples directly to the requirements of the drift chambers' design (the measurements of drift times). Nevertheless the optimization procedure is expensive, since once has to apply *two* complicated programs several times.

It is simpler and therefore more efficient to use indirect criteria for the optimal behaviour of the drift chamber, namely, criteria concerning only the electric field. Our experience has shown that the optimization of suitable functions constructed from the electric field values minimizes the asymmetry of the drift times.

At the end of this section the strip voltages determined to be optimal are presented. These voltages were obtained for 3050 V at the sense wires (SWs) and 1200 V at the potential wires (PWs), which were chosen

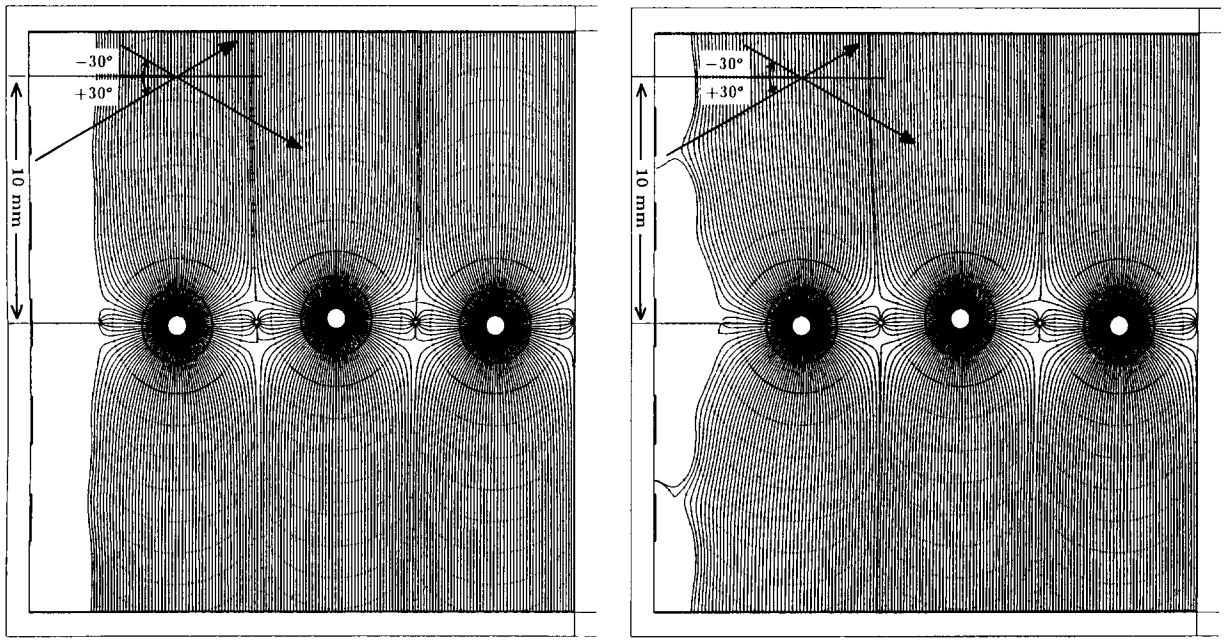

Fig. 10. Calculated development of the drift trajectories for optimized (left) and nonoptimized (right) voltages at the field-shaping strips. Both calculations are without a magnetic field.

to have a gas amplification in the desired order of magnitude. The strip voltages are

S3: 2400 V, S2/4: 1300 V, S1/5: 750 V.

Compared with voltages determined earlier (1987) experimentally for the same SW- and PW-voltages (S3: 1900 V, S2/4: 1070 V, S1/5: 625 V), a significantly higher level was obtained on all strips.

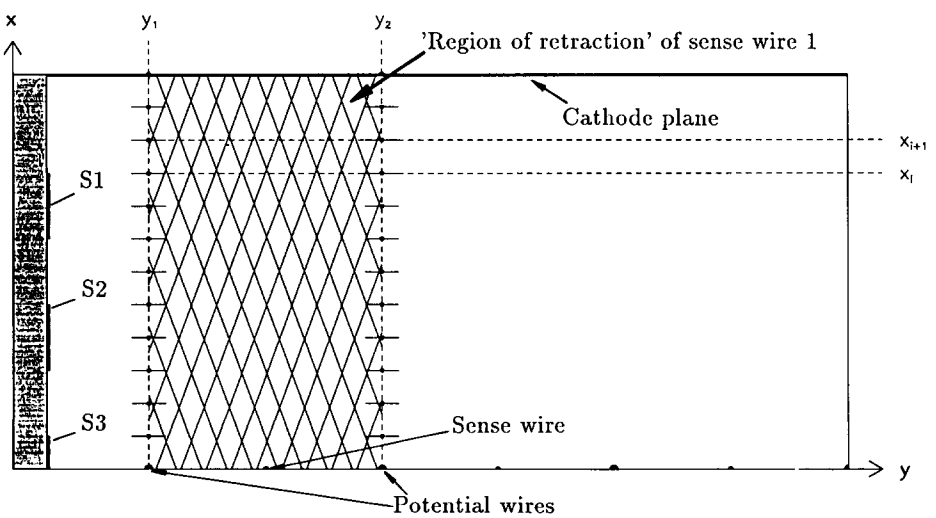

Fig. 11. The points used to define the function to be optimized by the program package PROFI; the 300 μm staggering of the sense wires (cf. fig. 2) is neglected in this connection.

2.3. Automatic voltage optimization

The construction of functions derived from the electric field values only enables to perform the optimization of the operating conditions of the drift chamber as a optimization problem concerning the electric field inside the drift chamber. In contrast to the optimization "by hand" the result can be obtained without using the program which simulates the electron drift.

Because of the symbolic input/output of the program package PROFI the optimization problem can be defined within this program structure and can be solved by *one* program run with "automatic" optimization. For an optimal drift process it is demanded that the electrostatic field is right/left symmetric with respect to a sense wire. In fig. 11 the "region of retraction" of sense wire 1 can be seen. Symmetric with respect to the line through the considered sense wire, perpendicular to the plane of the potential wires, 24 points were chosen, where the electric field is referenced. The points (x_i, y_1), $i = 1,\ldots,12$, are to the left of the sense wire, whereas the points (x_i, y_2), $i = 1,\ldots,12$, are placed to the right of the sense wire.

The function to be minimized is defined as

$$f(E) = \sum_{i=1}^{12} |E_y(x_i, y_1) + E_y(x_i, y_2)|. \quad (1)$$

If the electric field were optimal, the differences $E_y(x_i, y_1) - (-E_y(x_i, y_2)) = E_y(x_i, y_1) + E_y(x_i, y_2)$ should vanish. With the voltages 3050 V at the sense wires and 1200 V at the potential wires a minimization of this function leads to strip voltages of

S3: 2270 V, S2/4: 1425 V, S1/5: 685 V.

These values are similar to the "hand-made" ones and also significantly higher than the ones of 1987.

3. Measurements of the gas amplification

As outlined in section 1.4 the gas amplification at a sense wire is a measure for the electric field at the surface of the wire. It is obvious that equal surface fields at all sense wires are a necessary condition for an optimal electric field inside the drift cell; our calculations also have shown that this condition is sufficient.

3.1. Procedures of data taking and data reduction

To measure the (relative) gas amplifications at the six sense wires, one has to take a statistically significant number of events consisting of uniformly ionizing "particles" crossing a two-dimensional section (see fig. 2) of a FTD/RTD cell. After subtraction of the pedestals (cf. fig. 12), the average integral of the pulses arriving at one sense wire is proportional to the gas amplification if the amplifier used is charge conserving. The average pulse integrals at the six sense wires allow to compare the gas amplifications and therefore the surface fields of the sense wires.

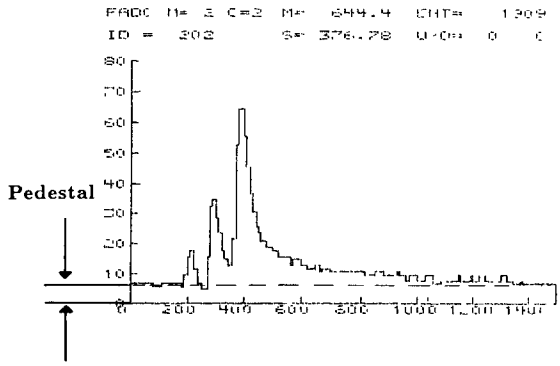

Fig. 12. A digitized drift cell pulse with three peaks. Also marked is the pedestal.

To suppress systematic errors, one has to select a subset of all events taken. The following criteria were used to define the cuts:

- Events with double- or multiple-tracks (as shown in fig. 12) were rejected,
- events with overflows were rejected,
- events with very small pulses were rejected, and
- events with oscillations [#3] in the trailing edge were rejected.

Two kinds of uniformly ionizing "particles" were used (details are explained in sections 3.2 and 3.3). All of the data have been taken without a magnetic field.

3.2. Electron beam data

First, a model of the original FTD/RTD cell [15,9,3] in a test beam of highly relativistic electrons (1.5 GeV/c) at the 2.5 GeV electron-synchrotron at Bonn University was used. These electrons were spread uniformly over the cell using a 6 mm lead block positioned in front of the cell.

5 runs with at least 8000 events each were performed; after applying the cut criteria described above, each run consisted of at least 3000 events.

The list of operating voltages used during the runs is displayed below. Since the test cell was old and affected by aging effects, it was not possible to run the higher, optimal strip voltages.

- Run 1, operating voltages: SW: 3050 V, PW: 1200 V, S3: 1900 V, S2/4: 1070 V, S1/5: 625 V. This was a set of nonoptimized voltages determined experimentally earlier (1987).
- Run 2, operating voltages: SW: 3125 V, PW: 1175 V,

[#3] These oscillations were caused by unstable amplifiers.

S3: 1500 V, S2/4: 1160 V, S1/5: 630 V. This was an experimental attempt to increase the gas amplifications.
- Run 3, operating voltages: SW: 2900 V, PW: 800 V, S3: 1450 V, S2/4: 1060 V, S1/5: 580 V. Since the test cell was not able to keep the high voltage required on S3, we tried to approach the optimal conditions by lowering the SW/PW voltages.
- Run 4, operating voltages: SW: 3050 V, PW: 1200 V, S3: 1350 V, S2/4: 1070 V, S1/5: 625 V. The maximum voltage level at S3 had decreased to 1350 V.
- Run 5, operating voltages: SW: 3050 V, PW: 1200 V, S3: 1200 V, S2/4: 1070 V, S1/5: 625 V. A further reduction of the voltage at strip S3 was required.

3.3. Laser data

Second, we employed the laser test cell and shot with a beam of a frequency-quadrupled neodymium–YAG laser at fixed position throughout the laser windows of the cell. The pulsed laser beam of wavelength 266 nm "simulates" a series of uniformly ionizing particles and is useful to measure the gas amplifications.

Using the laser, 4 runs with 8000 events each were performed. In contrast to the beam runs, we had only a few overflows, multiple tracks, or too small pulses. Therefore almost all of the events passed the cuts.

Again, the list of operating voltages used during the runs is displayed. Applying high voltages the laser test cell was much more stable than the test cell used for the beam runs. Therefore the hand-optimized voltages could be checked directly.
- Run 1, operating voltages: SW: 3050 V, PW: 1200 V, S3: 1900 V, S2/4: 1070 V, S1/5: 625 V. This was the set of nonoptimized voltages determined experimentally earlier (1987).
- Run 2, operating voltages: SW: 3050 V, PW: 1200 V, S3: 2400 V, S2/4: 1300 V, S1/5: 750 V. These were the voltages found with the hand-optimization described in section 2.2.
- Run 3, operating voltages: SW: 3050 V, PW: 1200 V, S3: 2400 V, S2/4: 1570 V, S1/5: 1125 V. This was another set of voltages [11], which has shown to be "overoptimized".
- Run 4, operating voltages: SW: 2800 V, PW: 1100 V, S3: 2200 V, S2/4: 1200 V, S1/5: 690 V. This was the voltage set of run 2 scaled down by a factor of 0.92. The aim of this run was to check whether the optimum field remains present under these conditions.

The voltages obtained by the automatic optimization were still not known at the time of the measurements and therefore could not be considered. Nevertheless the calculations have shown that there is no large difference between the surface fields obtained by the two optimization methods. Thus due to the minor effort involved the "automatic" numerical optimization should be preferred to the method also taking into account the drift times.

4. Comparison of calculations and measurements

4.1. Error sources and their treatment

While statistical errors were unimportant since we have taken a sufficient number of events per run, some systematic errors remained despite the cuts described in section 3.1. These errors yield wrong results for the gas amplifications that should be identical for the wire pairs 1 and 6, 2 and 5, and 3 and 4. The error sources are:
- Mechanical displacements of sense wires from the nominal position are possible (beam and laser runs). Small displacements of 10–20 μm, as one can expect, cause differences in the surface fields of the order of 1%. This results in a 10–15% effect for the gas amplifications.
- The amplifiers at the six channels might work differently (beam and laser runs). Measurements with test pulses have shown that because of this reason errors in the order of 5% have to be expected for the accuracy of the pulse integrals. This also carries through to the gas amplifications.
- Focussing–defocussing effects of the laser beam might occur (laser runs only). An ideal laser beam for calibration purposes has a constant cross section over the whole length of the test cell. This ideal case was not achieved during our test measurements. Thus the ionization density probably was not constant along the beam. The magnitude of this error was not estimated, but the larger errors for the laser runs compared to those of the beam runs were probably due to this reason.

The measured pulse integrals have been averaged by computing the mean value between equivalent wires (wires 1 and 6, wires 2 and 5, wires 3 and 4). The mean square deviation from the average then gives a measure of the quality of the considered run. For the comparison with the calculations we subsequently only dealt with the three averaged values.

4.2. Electron beam data

In fig. 13 a comparison between the measured pulse integrals and the calculated surface fields (2D) for the 5 beam runs is shown. The markers for the border wires (the wires closest to the field-shaping strips) are plotted filled, the other ones are plotted open. The errors for the different runs (determined as described above) appear in the legend, where the error bars have a run-dependent size. The error bars for the displayed data have a constant size, namely the average over the errors of the 5 runs.

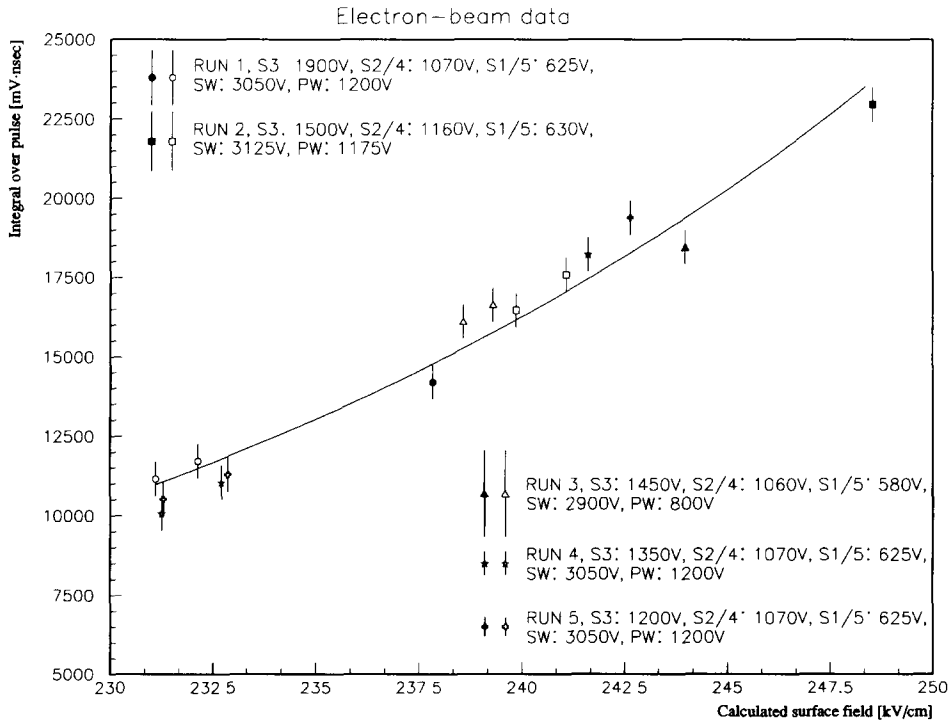

Fig. 13. The comparison between calculated surface fields and measured integrals of the pulses at the sense wires (beam data); for each run the marker for the wire closest to the field-shaping strips is filled.

We begin the discussion of the results with a remark on the global dependence between the calculated surface fields and the measured pulse integrals, which were our measure for the gas amplifications. Theoretically, an exponential dependence can be expected, which is visible (see the fitted exponential curve). More exactly, one should say there is no contradiction of the exponential shape of the curve; the range of the abscissa is too small to be able to state that the exponential curve is the only function which can be fitted.

The next point is the observation that the border wire 1 had the highest surface field/gas amplification in all runs. The reason for this was the fact that all beam runs were performed with too low voltages at the field-shaping strips, as explained in section 3.2. Additionally, the measurements confirm the numerical result that the voltages at the field-shaping strips have only little influence on the wires 2 and 3.

As supposed, run 3 was, with respect to optimal strip voltages, the best of all the runs performed. Run 2 had the highest level of surface fields/gas amplifications, which also was intended. Finally, the most important result is the comparison of runs 1, 4 and 5. The only difference between these runs was the (with increasing run number) decreasing potential at strip 3 (S3). In fig. 13 it can be seen that the surface fields/gas amplifications at wires 2 and 3 are close together for these runs, whereas the values for wire 1 withdraw from this group with decreasing potential on strip S3. One therefore can conclude indirectly that – as predicted by the calculations – the difference between the gas amplifications of the three sense wires is being reduced with increasing potential on strip S3.

4.3. Laser data

These data were generated with a laser beam crossing the 2D cell section of the laser test cell about 10 mm distant from the plane of the potential wires. Compared to the beam data, we had more freedom to choose the voltages (the cell was more stable at high voltages). On the other hand, we had larger errors, probably due to focussing–defocussing effects, as discussed in section 4.1.

The results are shown in fig. 14. The starting point again are the nonoptimized voltages of 1987. They show the same behaviour as with the beam data: the surface field/gas amplification at the border wire 1 is much larger than at wires 2 and 3.

Compared to that, the entries for the hand-optimized voltages (run 2) lie close together, for both calculations and measurements. This result confirms the correctness of the computational voltage optimization explicitly for the first time.

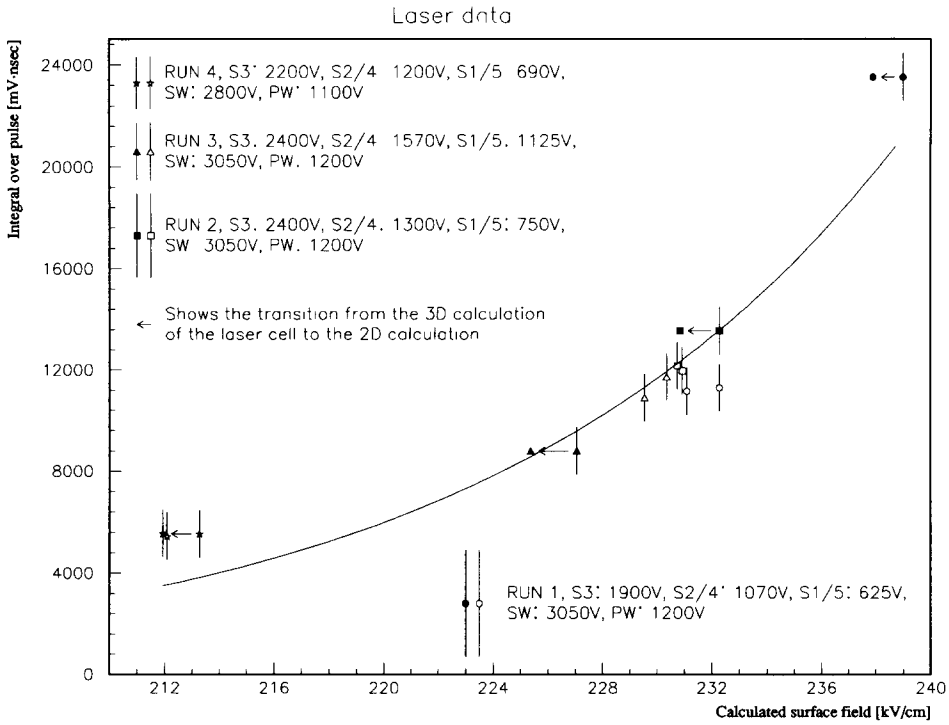

Fig. 14. The comparison between calculated surface fields and measured integrals of the pulses at the sense wires (laser data); for each run the marker for the wire closest to the field-shaping strips is filled.

Supporting the choice of these voltages is also the fact that a still higher level at the strip S3 than in run 3 is too much: This run is the only one where the gas amplification at wire 1 is lower than at wires 2 and 3 (in calculations as well as in measurements).

Finally, in run 4 it can be seen that a scale-down of the optimal voltages is possible without objections. This could become important if the final detector requires, after a longer duration of operation, lower voltages for safety reasons.

The global dependence between calculated surface fields and measured pulse integrals does not follow so well as the beam data follow the fitted exponential function. This could be caused by saturation effects.

4.4. The influence of the open boundary conditions (3D)

For fig. 14 it was required to calculate the three-dimensional electric field (cf. sections 1.3 and 2.1.2). The deviations from the 2D calculations are shown in fig. 14. The calculations for the old laser cell showed much larger deviations from the 2D calculations. These numerical results were one reason for a change of the cell geometry. This redesigning led to a laser test cell in which the deviations from the final FTD/RTD cell were negligible. See ref. [3] for details.

At the end of this paper another remark concerning the 1987 voltages (test runs 1): These voltages were determined experimentally in 1987 to be optimal for the old laser test cell (by measurements of gas amplifications). The large difference to the measurements presented in this paper is understandable using 3D calculations of the electrostatic field of the old laser cell. Using the 1987 voltages, they show almost equal surface fields at all sense wires. This is caused by the larger window of the old laser cell, as not supposed in 1987.

5. Conclusions

With this investigation the applicability of a numerical optimization for the operating voltages of the ZEUS forward drift chambers (which are representative of drift chambers with small drift cells) has been successfully tested.

The presence of dielectrics was incorporated into the calculations of the electrostatic field, and the influence on the drift times and the surface fields of the sense wires has proven not to be negligible.

Besides 2D calculations, 3D effects were taken into consideration (open boundary conditions). They also affect the drift times and surface fields in the test

chambers built and were required to be watched during the designing of the test chamber.

The field optimization was checked experimentally by measuring the gas amplifications at the six sense wires. A good agreement between calculations and measurements was observed.

As a general conclusion a reinforced usage of numerical methods while designing drift chambers can be recommended, especially under difficult experimental conditions.

Acknowledgements

This work was supported by DESY, Hamburg, and the HLRZ at the KFA, Jülich, with their IBM and CRAY vector computers. The authors also express their thanks to Mark Lomperski, who checked the draft version of the manuscript carefully for errors.

References

[1] M.P. Dobberstein, DESY M-89-01/BONN-IR-89-03 (1989).
[2] M.P. Dobberstein, DESY-F1-90-02 (1990).
[3] M.P. Dobberstein, Thesis, BONN-IR-90-51 (1990).
[4] St. Kramarczyk, Diploma Thesis, BONN-IR-89-36 (1989)
[5] F. Krawczyk and T. Weiland, DESY M-87-14 (1987).
[6] F. Krawczyk, Thesis, DESY-M-90-13 (1990).
[7] W. Müller et al., Archiv für Elektrotechnik 65 (1982) 299.
[8] W.-R. Novender, DESY M-88-02 (1988).
[9] Ch. Reineke, Diploma Thesis, BONN-IR-88-24 (1988).
[10] F. Sauli, CERN-77-09 (1977).
[11] M. Schäfer-Jotter and M.P. Dobberstein, private communication (1988).
[12] M. Schäfer-Jotter, Thesis (D 17), TH Darmstadt (1989).
[13] M. Schäfer-Jotter and W. Müller, IEEE Magnetics 26 (1990) 815.
[14] R. Stratmann, Diploma Thesis, BONN-IR-89-53 (1989).
[15] L. Weinsziehr, Diploma Thesis, BONN-IR-88-23 (1988).
[16] ZEUS Collaboration, The ZEUS Detector, Technical Proposal (1986).